

# Antiferromagnetic Kondo lattice in the layered compound $\text{CePd}_{1-x}\text{Bi}_2$ and comparison to the superconductor $\text{LaPd}_{1-x}\text{Bi}_2$

Fei Han,<sup>1</sup> Xiangang Wan,<sup>2</sup> Daniel Phelan,<sup>1</sup> Constantinos C. Stoumpos,<sup>1</sup> Mihai Sturza,<sup>1</sup> Christos D. Malliakas,<sup>1,3</sup> Qing'an Li,<sup>1</sup> Tian-Heng Han,<sup>1,4</sup> Qingbiao Zhao,<sup>1</sup> Duck Young Chung,<sup>1</sup> and Mercouri G. Kanatzidis<sup>1,3,\*</sup>

<sup>1</sup>Materials Science Division, Argonne National Laboratory, Argonne, Illinois 60439, USA

<sup>2</sup>National Laboratory of Solid State Microstructures, School of Physics, Collaborative Innovation Center of Advanced Microstructures, Nanjing University, Nanjing 210093, China

<sup>3</sup>Department of Chemistry, Northwestern University, Evanston, Illinois 60208, USA

<sup>4</sup>James Franck Institute and Department of Physics, University of Chicago, Chicago, Illinois 60637, USA

(Received 15 January 2015; revised manuscript received 9 June 2015; published 13 July 2015)

The layered compound  $\text{CePd}_{1-x}\text{Bi}_2$  with the tetragonal  $\text{ZrCuSi}_2$ -type structure was obtained from excess Bi flux. Magnetic susceptibility data of  $\text{CePd}_{1-x}\text{Bi}_2$  show an antiferromagnetic ordering below 6 K and are anisotropic along the  $c$  axis and the  $ab$  plane. The anisotropy is attributed to crystal-electric-field (CEF) effects and a CEF model which is able to describe the susceptibility data is given. An enhanced Sommerfeld coefficient  $\gamma$  of  $0.191 \text{ J mol Ce}^{-1} \text{ K}^{-2}$  obtained from specific-heat measurement suggests a moderate Kondo effect in  $\text{CePd}_{1-x}\text{Bi}_2$ . Other than the antiferromagnetic peak at 6 K, the resistivity curve shows a shoulderlike behavior around 75 K which could be attributed to the interplay between Kondo and CEF effects. Magnetoresistance and Hall-effect measurements suggest that the interplay reconstructs the Fermi-surface topology of  $\text{CePd}_{1-x}\text{Bi}_2$  around 75 K. Electronic structure calculations reveal that the Pd vacancies are important to the magnetic structure and enhance the CEF effects which quench the orbital moment of Ce at low temperatures.

DOI: [10.1103/PhysRevB.92.045112](https://doi.org/10.1103/PhysRevB.92.045112)

PACS number(s): 75.30.Mb, 71.55.-i, 71.20.Eh, 72.15.Qm

## I. INTRODUCTION

Ce-based intermetallics exhibit a wide range of novel behaviors such as magnetic ordering, Kondo effect, heavy-fermion behavior, and superconductivity. These phenomena arise from the competition between Ruderman-Kittel-Kasuya-Yosida (RKKY) and Kondo interactions and can be described using the Kondo-lattice model (the so-called Doniach phase diagram) [1]. When the ground state is dominated by the Kondo interaction, the system is nonmagnetic due to the Kondo effect, for instance in  $\text{CeCu}_6$  [2]. When the ground state is dominated by the RKKY interaction, the system orders magnetically. When the strengths of these two interactions are comparable, the ground state is Kondo type but still magnetic.  $\text{CeAl}_2$  and  $\text{CeB}_6$  are typical examples of Kondo-type antiferromagnets [3,4].

Recently, we reported that  $\text{LaPd}_{1-x}\text{Bi}_2$  is a superconductor below 2.1 K, while the isostructural compound  $\text{CePd}_{1-x}\text{Bi}_2$  has an antiferromagnetic (AFM) transition at 6 K [5]. In this article, we present detailed magnetic and transport properties, and theoretical calculations for  $\text{CePd}_{1-x}\text{Bi}_2$ , which shows the anisotropy of antiferromagnetism and the presence of Kondo and crystal-electric-field (CEF) effects in this material. The interplay between the Kondo and CEF effects governs the transport behavior of  $\text{CePd}_{1-x}\text{Bi}_2$  between its Neel temperature ( $T_N$ ) and 75 K at which the Fermi surface is obviously reconstructed by the interplay. These results indicate that  $\text{CePd}_{1-x}\text{Bi}_2$  is a Kondo-lattice antiferromagnet.

## II. EXPERIMENTAL DETAILS

Single-crystalline  $\text{CePd}_{1-x}\text{Bi}_2$  was grown using bismuth flux [6]. The starting materials Ce, Pd, and Bi with the mole

ratio 1:1:12 and the total mass 3 g were weighed, mixed, and placed in an alumina crucible. All handling was performed in a glove box with a protective argon atmosphere (both  $\text{H}_2\text{O}$  and  $\text{O}_2$  are limited below 0.1 ppm). Then the alumina crucible was jacketed by an evacuated silica tube. The tube was heated to  $900^\circ\text{C}$  in a box furnace and kept at  $900^\circ\text{C}$  for 10 h. A slow-cooling process at the rate  $5^\circ\text{C/h}$  was carried out from  $900^\circ\text{C}$  to  $500^\circ\text{C}$ , and at  $500^\circ\text{C}$  the excess Bi flux was removed by centrifugation [7]. The obtained crystals were shiny silver-color plates with a typical dimension of  $5 \times 5 \times 0.5 \text{ mm}$  and stable in the air.

Single-crystal x-ray diffraction (SCXRD) was carried out on a STOE diffractometer. Data reduction was performed with the software X-AREA [8], and the structure was solved by direct methods using the SHELXTL software [9]. The resulting structure parameters are listed in Table I.

The magnetic susceptibility data for  $\text{CePd}_{1-x}\text{Bi}_2$  were collected with a superconducting quantum interference device (SQUID) in a Quantum Design Magnetic Property Measurement System (MPMS-3).

Thermodynamics and transport measurements including specific heat, resistivity, magnetoresistance, and Hall effect were done on the Quantum Design Physical Property Measurement System (PPMS). We employed the thermal-relaxation technique [10] to perform the specific-heat measurements. Resistivity, magnetoresistance, and Hall-effect measurements were simultaneously carried out using a six-probe geometry [11].

## III. EXPERIMENTAL DATA AND DISCUSSION

### A. Crystal structure

Figure 1(a) shows a typical platelike crystal of  $\text{CePd}_{1-x}\text{Bi}_2$ . The compound adopts the tetragonal  $\text{ZrCuSi}_2$ -type structure and features partial occupancy of Pd atoms as determined

\*m-kanatzidis@northwestern.edu

TABLE I. Crystal and structure refinement data at room temperature for  $\text{CePd}_{1-x}\text{Bi}_2$ .

Empirical formula	$\text{CePd}_{0.78(2)}\text{Bi}_2$
Formula weight	641.07
Crystal system	Tetragonal
Space group	$P4/nmm$
Unit cell dimensions	$a = 4.6136(19) \text{ \AA}$ , $\alpha = 90^\circ$ $b = 4.6136(19) \text{ \AA}$ , $\beta = 90^\circ$ $c = 9.650(6) \text{ \AA}$ , $\gamma = 90^\circ$
Volume	$205.39(17) \text{ \AA}^3$
Z	2
Density (calculated)	$10.366 \text{ g/cm}^3$
Absorption coefficient	$99.419 \text{ mm}^{-1}$
F(000)	520
Reflections collected	609
Independent reflections	134 [ $R_{\text{int}} = 0.1016$ ]
Completeness to $\theta = 24.92^\circ$	97.8%
Refinement method	Full-matrix least-squares on $F^2$
Data/restraints/parameters	134/0/12
Goodness-of-fit	1.031
Final R indices [ $>2\sigma(I)$ ]	$R_{\text{obs}} = 0.0388$ , $wR_{\text{obs}} = 0.0579$
R indices (all data)	$R_{\text{all}} = 0.0538$ , $wR_{\text{all}} = 0.0602$
Largest diff. peak and hole	2.410 and $-2.922 \text{ e \AA}^{-3}$
Atomic coordinates:	
Ce	$2c [\frac{1}{4}, \frac{1}{4}, 0.2687(3)]$ Occupancy = 1, $U_{\text{eq}} = 0.0013(1)$
Pd	$2b [\frac{3}{4}, \frac{1}{4}, \frac{1}{2}]$ Occupancy = 0.78(2), $U_{\text{eq}} = 0.0014(2)$
Bi	$2a [\frac{3}{4}, \frac{1}{4}, 0]$ Occupancy = 1, $U_{\text{eq}} = 0.0015(1)$
Bi	$2c [\frac{1}{4}, \frac{1}{4}, 0.6593(2)]$ Occupancy = 1, $U_{\text{eq}} = 0.0018(1)$

by single-crystal x-ray diffraction, shown in Fig. 1(b). The composition was refined as  $\text{CePd}_{0.78(2)}\text{Bi}_2$  after the diffraction data are corrected for absorption using an analytical expression. In the structure, the  $\text{Pd}_{1-x}\text{Bi}$  layer adopts the same anti-PbO-type structure as the FeAs layer in the iron-based superconductors [12,13], while the additional Bi atoms form an extended Bi square net. Reciprocal space reconstruction of single-crystal x-ray diffraction data from a  $\text{CePd}_{0.78(2)}\text{Bi}_2$  crystal is shown in Fig. 1(c). The  $(hk0)$  reflections are very sharp, indicating excellent crystalline quality. Extra reflections corresponding to superstructures were not observed in reciprocal space, suggesting that the Pd vacancy defects are randomly disordered in the structure.

### B. Magnetic properties

The molar magnetic susceptibilities  $\chi(T)$  collected with the field applied along the  $c$  axis and the  $ab$  plane, respectively, and their inverses  $1/\chi$  are shown in Fig. 2 and its inset, respectively. Large anisotropy is observed in  $\text{CePd}_{0.78(2)}\text{Bi}_2$ : On one hand, the magnitude of magnetic susceptibility in two directions is different, especially at low temperatures. On the other hand, when the field is parallel to the  $c$  axis, a sharp peak is observed at 6 K, indicating an AFM ordering of the Ce moments, but when the field is parallel to the  $ab$  plane no peak is found. Similar behavior was observed in  $\text{CeNi}_{0.8}\text{Bi}_2$  [14], suggesting

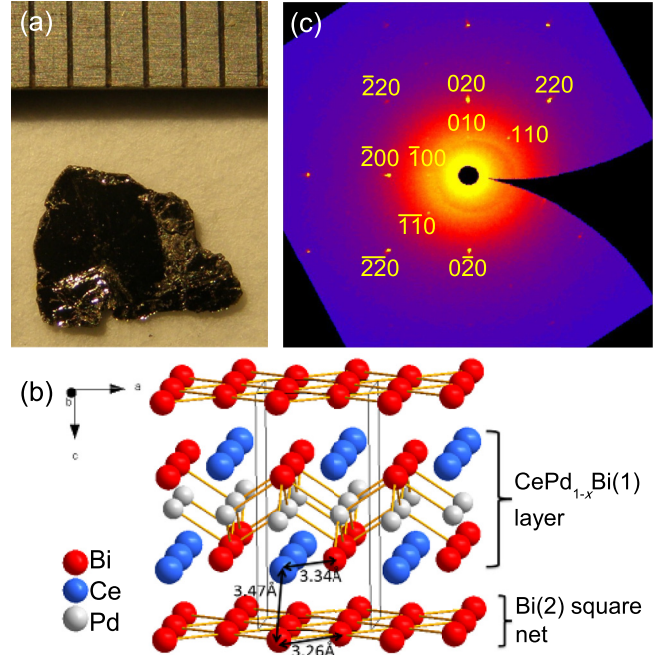


FIG. 1. (Color online) (a) Photograph of a typical  $\text{CePd}_{0.78(2)}\text{Bi}_2$  crystal. (b) Layered crystal structure of  $\text{CePd}_{0.78(2)}\text{Bi}_2$ . (c) Reciprocal space reconstruction of single-crystal x-ray diffraction data from a  $\text{CePd}_{0.78(2)}\text{Bi}_2$  crystal.

that the magnetic structure of  $\text{CePd}_{0.78(2)}\text{Bi}_2$  is similar to that of  $\text{CeNi}_{0.8}\text{Bi}_2$  [15]. The anisotropy of magnetic susceptibility persists up to the highest temperature measured (300 K). This anisotropy doubtless reflects a high-lying crystal-field doublet ( $\Delta/k_B > 300 \text{ K}$ ) which might arise from strong anisotropy in the  $4f$ -conduction hybridization.

We tentatively fit the susceptibility data in two directions with the Curie-Weiss law,

$$\chi = \frac{C}{T - \Theta_p}. \quad (1)$$

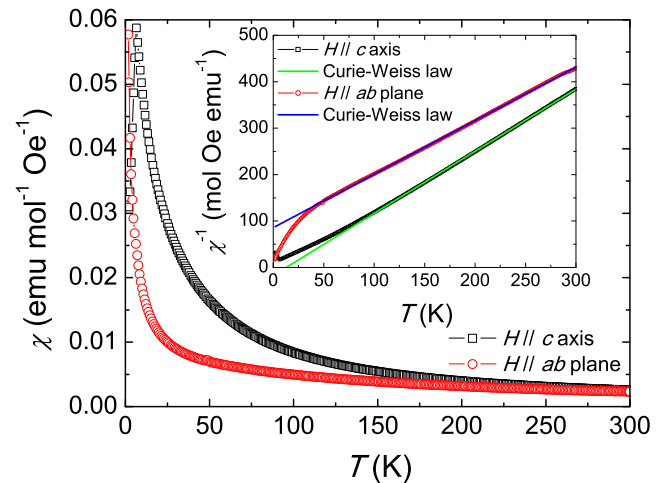


FIG. 2. (Color online) Temperature dependence of magnetic susceptibilities  $\chi(T)$  (main plot) and their inverses  $1/\chi$  (inset) for  $\text{CePd}_{0.78(2)}\text{Bi}_2$  with the field applied along the  $c$  axis and the  $ab$  plane, respectively.

From the fitting procedure, we get the paramagnetic Curie temperatures  $\Theta_p = 12.8$  K (when  $H \parallel c$ ) and  $-74.7$  K (when  $H \parallel ab$ ), the effective magnetic moments  $\mu_{\text{eff}} = 2.45 \mu_B/\text{Ce}$  (when  $H \parallel c$ ) and  $2.63 \mu_B/\text{Ce}$  (when  $H \parallel ab$ ). The observed values of  $\mu_{\text{eff}}$  are very close to what one would expect for a free  $\text{Ce}^{3+}$  ion ( $2.54 \mu_B/\text{Ce}$ ), indicating that the magnetic moment comes from the trivalent Ce ion state. The deviation from the Curie-Weiss behavior below 100 K (when  $H \parallel c$ ) and 50 K (when  $H \parallel ab$ ), respectively, can be attributed to the CEF effect on the ground state.

For a tetragonal point symmetry,  $4mm$  ( $C_{4v}$ ), at the Ce site, the CEF Hamiltonian can be written [16] as

$$H_{\text{CEF}} = B_2^0 O_2^0 + B_4^0 O_4^0 + B_4^4 O_4^4, \quad (2)$$

where  $B_n^m$  are the CEF parameters which can be determined from the experimental data, and  $O_n^m$  are Stevens operator equivalents obtained using the angular momentum operators [17–19].

For  $\text{Ce}^{3+}$ , the Hund's rule multiplet is  $J = \frac{5}{2}$ , and we have diagonalized the Hamiltonian described by Eq. (2) using a basis of the six  $|m_j\rangle$  states ( $|\frac{5}{2}\rangle$ ,  $|\frac{3}{2}\rangle$ ,  $|\frac{1}{2}\rangle$ ,  $|\frac{1}{2}\rangle$ ,  $|\frac{3}{2}\rangle$ ,  $|\frac{5}{2}\rangle$ ). The Hamiltonian splits the levels into three Kramer's doublets. The eigenvectors were then employed to determine the molar magnetic susceptibility with the field parallel ( $\chi_c$ ) and perpendicular ( $\chi_{ab}$ ) to the  $c$  axis. We assume that the measured magnetic susceptibility contains contributions from the crystal-field states ( $\chi_i^{\text{cf}}$ ) and the molecular field ( $\lambda_i$ ) [16,20], such that

$$\frac{1}{\chi_c} = \frac{1}{\chi_c^{\text{cf}}} - \lambda_c, \quad (3)$$

$$\frac{1}{\chi_{ab}} = \frac{1}{\chi_{ab}^{\text{cf}}} - \lambda_{ab}. \quad (4)$$

Formulas for  $\chi_c$  and  $\chi_{ab}$  can be found in [20,21] and references therein, which we list here for convenience:

$$\chi_c = (g_J \mu_B)^2 \frac{N_A}{Z} \sum_n \exp\left(\frac{-E_n}{kT}\right) \left[ \frac{|\langle n | J_z | n \rangle|^2}{kT} + 2 \sum_{m \neq n} \frac{|\langle n | J_z | m \rangle|^2}{E_m - E_n} \right], \quad (5)$$

$$\chi_{ab} = (g_J \mu_B)^2 \frac{N_A}{Z} \sum_n \exp\left(\frac{-E_n}{kT}\right) \left[ \frac{|\langle n | J_x | \tilde{n} \rangle|^2}{kT} + 2 \sum_{m \neq n, \tilde{n}} \frac{|\langle n | J_x | m \rangle|^2}{E_m - E_n} \right]. \quad (6)$$

Here,  $|n\rangle$  and  $|m\rangle$  represent eigenstates of  $H_{\text{CEF}}$ ,  $|\tilde{n}\rangle$  is the Kramer's conjugate wave function of  $|n\rangle$ ,  $g_J$  is the Lande  $g$  factor,  $\mu_B$  is the Bohr magneton,  $N_A$  is Avogadro's number,  $Z$  is the partition function for the eigenstates of  $H_{\text{CEF}}$ ,  $E_n$  represents the energy level of  $|n\rangle$ , and  $J_z$  and  $J_x$  are the operators for the  $z$  and  $x$  components of the total angular momentum.

The value of  $B_2^0$  can be determined using the high-temperature expansion of the magnetic susceptibility [17–19],

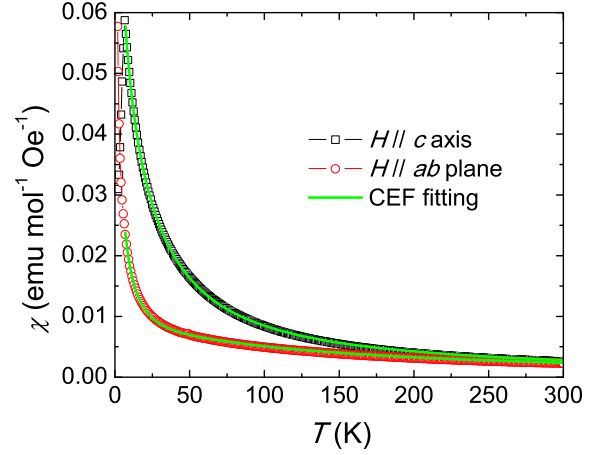


FIG. 3. (Color online) Fit to the magnetic susceptibility data based on the CEF model.

which gives  $B_2^0$  as

$$B_2^0 = \frac{10}{3} \frac{\Theta_{ab} - \Theta_c}{(2J-1)(2J+3)}. \quad (7)$$

Here,  $\Theta_{ab}$  represents the paramagnetic Curie-Weiss temperature in the direction of the  $ab$  plane and  $\Theta_c$  in the direction of the  $c$  axis. It should be noted that Eq. (7) above is only valid for isotropic exchange interactions (i.e., isotropic molecular field parameters).

Taking the values of  $\Theta_{ab} = -74.7$  K and  $\Theta_c = 12.8$  K obtained in the fitting procedure of Curie-Weiss behavior into the above Eq. (7), we get  $B_2^0 = -9.11$  K ( $-0.785$  meV). However, with  $B_2^0 = -9.11$  K fixed and  $B_4^0$ ,  $B_4^4$  varied, fits to the magnetic susceptibility data were not optimal. This indicates that the anisotropic magnetic exchanges and hence the  $B_2^0$  value estimated above are not valid.

Then we allowed  $B_2^0$ ,  $B_4^0$ , and  $B_4^4$  to vary and optimization of the crystal-field parameters yielded an excellent fit to the susceptibilities along both directions, as shown in Fig. 3. The obtained crystal-field parameters were  $B_2^0 = -4.79$ ,  $B_4^0 = -0.74$ , and  $B_4^4 = 4.96$  K, while the values of  $\lambda_{ab}$  and  $\lambda_c$  were  $-14.65$  and  $-10.01$   $\text{emu}^{-1} \text{mol Oe}$ , respectively. Note that the magnitudes of the obtained parameters were comparable to those reported from  $\text{CeNi}_{0.8}\text{Bi}_2$  [14]. The wave functions and energies of the obtained states are listed in Table II.

TABLE II. Energy-level schemes, and the corresponding wave functions for  $\text{CePd}_{1-x}\text{Bi}_2$ .

Energy	$ \frac{5}{2}\rangle$	$ \frac{3}{2}\rangle$	$ \frac{1}{2}\rangle$	$ \frac{1}{2}\rangle$	$ \frac{3}{2}\rangle$	$ \frac{5}{2}\rangle$
361 K	-0.406	0	0	0	-0.914	0
361 K	0	-0.914	0	0	0	-0.406
100 K	0	0	1	0	0	0
100 K	0	0	0	1	0	0
0 K	0.914	0	0	0	-0.406	0
0 K	0	-0.406	0	0	0	-0.914

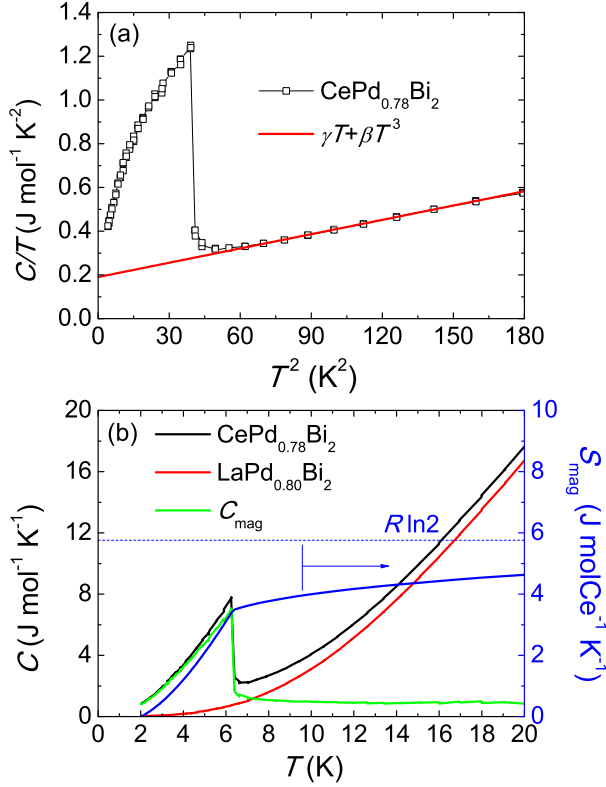


FIG. 4. (Color online) (a) Specific heat divided by temperature  $C/T$  for  $\text{CePd}_{0.78(2)}\text{Bi}_2$  as a function of  $T^2$ . Red line shows a linear fit to the data above  $T_N$ . The slope and intercept of the red line represent  $\beta$  and  $\gamma$ , respectively. (b) Specific heat  $C$  vs temperature  $T$  for  $\text{CePd}_{0.78(2)}\text{Bi}_2$  and its nonmagnetic phonon reference compound  $\text{LaPd}_{0.80(2)}\text{Bi}_2$ . After the specific heat of  $\text{LaPd}_{0.80(2)}\text{Bi}_2$  is subtracted from that of  $\text{CePd}_{0.78(2)}\text{Bi}_2$ , the magnetic contribution to the specific heat  $C_{\text{mag}}$  is obtained and leads to a magnetic entropy  $S_{\text{mag}}$ .

### C. Specific heat

The AFM transition at 6 K is reconfirmed by the sharp peak observed in the specific heat of  $\text{CePd}_{0.78(2)}\text{Bi}_2$  as a function of temperature, as shown in Figs. 4(a) and 4(b). By neglecting the contribution of fluctuating magnons above  $T_N$ , the specific heat can be separated into electronic and phonon parts:  $\gamma T$  and  $\beta T^3$ . The  $C/T \sim T^2$  curve is well fitted in a linear relationship in Fig. 4(a). In other words, the part of  $T_N < T < \sqrt{180}$  of the experimental specific-heat data can be well described with the formula

$$\frac{C}{T} = \gamma + \beta T^2. \quad (8)$$

From the fitting, we estimate  $\gamma$  and  $\beta$  to be  $0.191 \text{ J mol Ce}^{-1} \text{ K}^{-2}$  and  $0.00218 \text{ J mol Ce}^{-1} \text{ K}^{-4}$ , respectively.

The value of the Sommerfeld coefficient  $\gamma$  reflects a large effective mass of electrons and suggests a moderate heavy-fermion behavior, or Kondo effect. Taking  $\beta = 0.00218 \text{ J mol Ce}^{-1} \text{ K}^{-4}$  in the formula

$$\Theta_D = \left( \frac{12\pi^4 N R}{5\beta} \right)^{\frac{1}{3}}, \quad (9)$$

we can obtain the Debye temperature  $\Theta_D = 150 \text{ K}$ . Here,  $N$  refers to the number of atoms in the chemical formula and  $R$  is the gas constant.

In Fig. 4(b), the specific-heat data of a nonmagnetic phonon reference compound  $\text{LaPd}_{0.80(2)}\text{Bi}_2$  are also plotted. (The  $\text{LaPd}_{0.80(2)}\text{Bi}_2$  crystal used for the specific-heat measurement does not have bulk superconductivity above 2 K.) Subtracting the specific heat of the reference compound  $\text{LaPd}_{0.80(2)}\text{Bi}_2$  from that of  $\text{CePd}_{0.78(2)}\text{Bi}_2$ , as shown in Fig. 4(b), we can get the magnetic contribution (green line) to the specific heat and calculate the magnetic entropy (blue line) using the integral

$$S_{\text{mag}} = \int \frac{C_{\text{mag}}}{T} dT. \quad (10)$$

The magnitude of the specific-heat jump associated with the AFM transition is  $\approx 7 \text{ J mol Ce}^{-1} \text{ K}^{-1}$ , which is higher than that of  $\text{CeNi}_{1-x}\text{Bi}_2$  [22], and is used to calculate the Kondo temperature  $T_K$  later on. At  $T_N$ , the magnetic entropy is  $3.45 \text{ J mol Ce}^{-1} \text{ K}^{-1}$ , which reaches 60 percent of the theoretical  $R \ln 2 = 5.76 \text{ J mol Ce}^{-1} \text{ K}^{-1}$ , where  $R \ln 2$  represents the entropy of the doublet ground state of  $\text{Ce}^{3+}$  ions. Kondo compounds with a magnetic ground state show less ordering of spins due to the suppressing effect of the Kondo interaction on the RKKY interaction. This degenerate magnetic ground state accounts for the reduced experimental magnetic entropy at  $T_N$  [23,24].

To estimate the Kondo temperature  $T_K$  of  $\text{CePd}_{0.78(2)}\text{Bi}_2$ , we used the method described by Bredl *et al.* [25], where in the mean-field approach the heat capacity jump  $\Delta C_{\text{mag}}$  of a Kondo-lattice compound is related to its Kondo temperature. The expression of  $\Delta C_{\text{mag}}$  is

$$\Delta C_{\text{mag}} = \frac{6N_A k_B}{\psi'''(\frac{1}{2} + x)} \left[ \psi' \left( \frac{1}{2} + x \right) + x \psi'' \left( \frac{1}{2} + x \right) \right]^2, \quad (11)$$

where  $x = (T_K/T_N)/2\pi$  and  $\psi'$ ,  $\psi''$ , and  $\psi'''$  are the first, second, and third derivative of the polygamma function, respectively, and  $N_A$  and  $k_B$  are Avogadro's number and the Boltzmann constant, respectively. A plot of  $\Delta C_{\text{mag}}$  versus

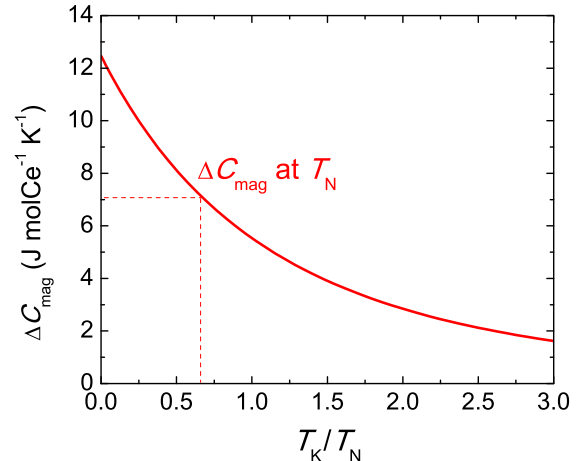


FIG. 5. (Color online) Estimation of the Kondo temperature from the heat capacity jump of magnetic transition.

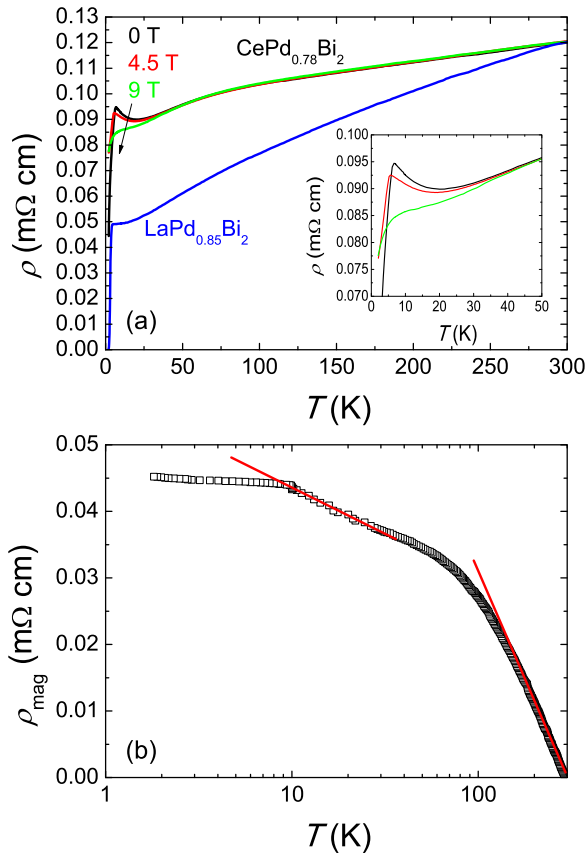


FIG. 6. (Color online) (a) In-plane resistivity of  $\text{CePd}_{0.78(2)}\text{Bi}_2$  and superconducting  $\text{LaPd}_{0.85(2)}\text{Bi}_2$ . The fields were applied parallel to the  $c$  axis.

$T_K/T_N$  is shown in Fig. 5, from which we can conclude that the Kondo temperature for  $\text{CePd}_{0.78(2)}\text{Bi}_2$  is 4.0 K.

#### D. Resistivity

The temperature dependence of resistivity for  $\text{CePd}_{0.78(2)}\text{Bi}_2$  is shown in Fig. 6(a). Above 75 K, the zero-field resistivity shows a linear behavior and is weakly dependent on temperature. The weak dependence reflects a strong scattering effect in the conductive layers. The strong scattering effect could be attributed to the Pd vacancy defects in the  $\text{Pd}_{1-x}\text{Bi}$  layer. The large number of Pd vacancies can be thought of as nonmagnetic impurities and plays the role of scattering centers. Around 75 K, the zero-field resistivity turns down gradually and then rises again at 20 K, forming a broad shoulder at 75 K and a resistivity minimum at 20 K. The minimum at 20 K is a typical Kondo-type response in resistivity. At 6 K, a sharp peak corresponding to the AFM transition is observed. The broad shoulder is possibly associated with the interplay between Kondo and CEF effects as found in some other Ce-based compounds such as  $\text{CeNiX}_2$  ( $X = \text{Si, Ge, Sn}$ ),  $\text{Ce}_2\text{T}_3\text{Ge}_5$  ( $T = \text{Ni, Rh, Ir}$ ), and  $\text{CeNiBi}_2$  [26–29]. At the field of 4.5 and 9 T, the peak at  $T_N$  vanishes and shifts to lower temperatures gradually as the upturn of resistivity is also suppressed. This means the AFM ordering can be suppressed to lower temperatures and even quenched by high fields.

The resistivity of superconducting  $\text{LaPd}_{0.85(2)}\text{Bi}_2$  is also plotted in Fig. 6(a). The magnetic contribution to the resistivity  $\rho_{\text{mag}}$  can be obtained by subtracting the resistivity of  $\text{LaPd}_{0.85(2)}\text{Bi}_2$  from that of  $\text{CePd}_{0.78(2)}\text{Bi}_2$ . In Fig. 6(b),  $\rho_{\text{mag}}$  is plotted as a function of  $\ln T$ .  $\rho_{\text{mag}}$  is almost linear with  $\ln T$  in two different temperature regions, which are separated by a hump at about 75 K. According to the model of Cornut and Coqblin [30], such a behavior can be expected for a Kondo-type interaction in the presence of crystal fields. The linear behaviors in two different temperature regions represent the Kondo scattering in the crystal-field ground state and in the whole multiplet of the  $J = \frac{5}{2}$  state, respectively. The hump at 75 K can be considered as the energy of the overall crystal-field splitting.

#### E. Magnetoresistance

Magnetoresistance (MR) is a powerful tool to investigate the electronic scattering process. Here, MR is expressed as

$$\Delta\rho = \frac{\rho(H) - \rho_0}{\rho_0}, \quad (12)$$

where  $\rho(H)$  and  $\rho_0$  represent the longitudinal resistivity at a magnetic field  $H$  and that at zero field, respectively. The field dependences of MR at temperatures near or above 75 K are shown in Fig. 7(a), while those below 75 K are shown in Fig. 7(b). The curves in Fig. 7(b) reveal a rather different feature compared to those in Fig. 7(a). When  $T \geq 75$  K, the MR is positive and exhibits a linear relationship with  $H$ . In sharp contrast, when  $T < 75$  K, the MR becomes negative and exhibits a clear nonlinear dependence. The abnormal behavior at 5 K is attributed to the presence of AFM ordering. Collecting all the MR values at 9 T, we plot them as a function of temperature in Fig. 7(c). One can see the MR is positive in sign and small in value at or above 75 K, and below 75 K the MR versus  $T$  curve diverges to the negative area and then increases rapidly in absolute value. The dramatic evolution of MR shows that the scattering effect changes from conventional lattice scattering and impurity scattering (above 75 K) to a more complex scattering (below 75 K), which could be caused by the gradual emergence of the heavy-fermion behavior or CEF splitting, or both.

The semiclassical transport theory predicts that Kohler's rule should be satisfied for a single-band metal with an isotropic Fermi surface [31]. Sometimes this rule is also applicable for a multiband system when the number of charge carriers from each band is independent of temperature and the scattering rates of different bands have a similar temperature dependence [32]. Kohler's rule can be written as

$$\frac{\Delta\rho}{\rho_0} = F\left(\frac{\mu_0 H}{\rho_0}\right). \quad (13)$$

This equation means that the  $\Delta\rho/\rho_0$  versus  $\mu_0 H/\rho_0$  curves for different temperatures, the so-called Kohler's plot, should be scaled to a universal curve if the rule is obeyed. The scaling based on the Kohler's plot for our sample is shown in Fig. 7(d). It is obvious that Kohler's rule is violated in our system, indicating that  $\text{CePd}_{0.78(2)}\text{Bi}_2$  is a multiband system and the carrier contribution from each band varies with temperature.

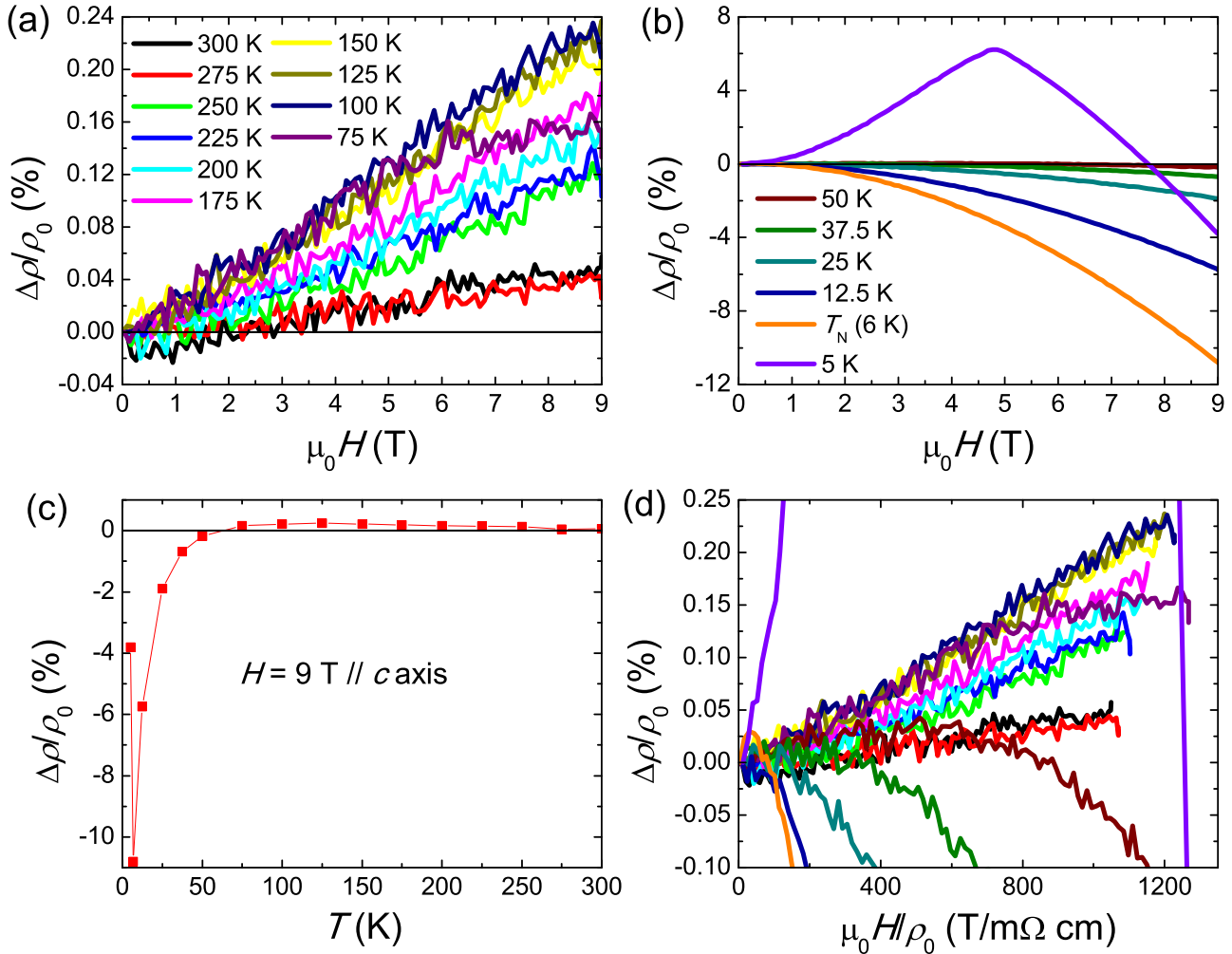


FIG. 7. (Color online) Field dependence of magnetoresistance (MR) for CePd<sub>0.78(2)</sub>Bi<sub>2</sub> with (a)  $T \geq 75$  K and (b)  $T < 75$  K. (c) Temperature dependence of MR for CePd<sub>0.78(2)</sub>Bi<sub>2</sub> at the field of 9 T. (d) The Kohler's plot of MR.

### F. Hall effect

The Hall coefficient measured on CePd<sub>0.78(2)</sub>Bi<sub>2</sub> is displayed in Fig. 8. Above 75 K, the Hall coefficient  $R_H$  remains nearly temperature independent and converges to  $-1.65 \times 10^{-4}$  cm<sup>3</sup>/C, which is consistent with the negligible positive MR and the linear behavior in resistivity above 75 K. A rough estimate from the single-band model leads to a carrier density of  $3.8 \times 10^{22}$ /cm<sup>3</sup> at these temperatures, while the negative sign of the Hall coefficient indicates that above 75 K, the transport of CePd<sub>0.78(2)</sub>Bi<sub>2</sub> is dominated by electrons. Deviation from linearity and sign reversal is observed below 75 K in the Hall coefficient versus temperature ( $R_H$  vs  $T$ ) function.

It is worth noting that the superconducting LaPd<sub>0.85(2)</sub>Bi<sub>2</sub> has an almost constant Hall coefficient of  $-1.7 \times 10^{-4}$  cm<sup>3</sup>/C from 2 to 300 K, over the whole temperature region [5]. In addition, LaPd<sub>0.85(2)</sub>Bi<sub>2</sub> does not exhibit the shoulderlike behavior but is nearly linear all the way in resistivity [5]. The close Hall coefficient and the similar linear behavior of resistivity between CePd<sub>0.78(2)</sub>Bi<sub>2</sub> above 75 K and LaPd<sub>0.85(2)</sub>Bi<sub>2</sub> from 2

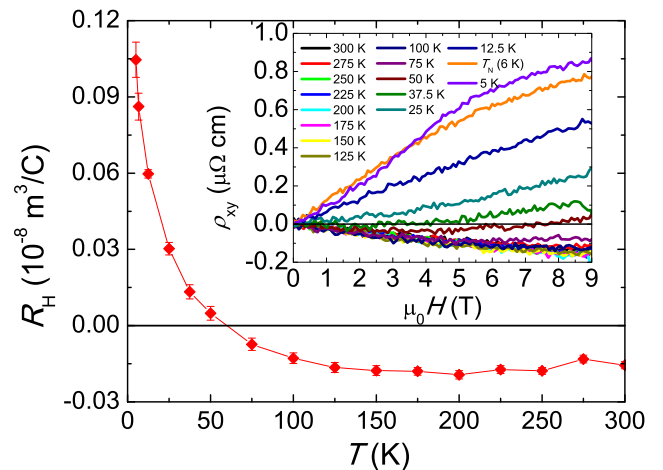


FIG. 8. (Color online) Temperature dependence of Hall coefficient  $R_H$  for CePd<sub>0.78(2)</sub>Bi<sub>2</sub> measured with the field perpendicular to the  $ab$  plane. Inset: Hall resistivity  $\rho_{xy}$  vs magnetic field  $\mu_0 H$  at different temperatures.

to 300 K suggest that from 75 and 300 K,  $\text{CePd}_{0.78(2)}\text{Bi}_2$  and  $\text{LaPd}_{0.85(2)}\text{Bi}_2$  have a similar Fermi surface that does not vary in this temperature region. However, below 75 K, the interplay between Kondo and CEF effects in  $\text{CePd}_{0.78(2)}\text{Bi}_2$  obviously reconstructs its Fermi-surface topology. The partial gap of the Fermi surfaces removes the density of states on some Fermi pockets and may leave one of the hole pockets partially or fully ungapped.

### G. Theoretical calculations

To gain a fuller understanding of the physical properties, we also performed density-functional theory (DFT) calculations based on the local density approximation (LDA) with the full-potential, all-electron, linear muffin-tin-orbital method [33]. We used the LDA+ $U$  scheme [34] to approximate the localized nature of the Ce 4*f* electrons and took the  $U = 7.5$  eV and  $J = 0.68$  eV [35]. We included spin-orbit (SO) coupling interactions, which play an important role in this compound.

We performed calculations for several magnetic arrangements, including ferromagnetic (FM); with interplane AFM coupling and intraplane FM coupling (A-AFM); with lines of Ce ions coupled ferromagnetically in a given direction [100] but with alternate lines having opposite spin orientation (C-AFM); and with Ce ions coupled antiferromagnetically with all of their nearest neighbors (G-AFM). To account for the possible magnetic anisotropy, we carried out calculations with magnetization aligning along the [100], [110], [111], and [001] directions, respectively. Our calculations reveal an A-AFM magnetic ground-state configuration of  $\text{CePdBi}_2$ ; however the numerical magnetic easy axis is [110], which is different from our experimental results. We present the density of state (DOS) of  $\text{CePdBi}_2$  in Fig. 9(a). As shown in this figure, the Ce-4*f* state is quite narrow and located far from the Fermi energy. The Pd-4*d* states mainly disperse from  $-4.5$  eV to Fermi level, while the Bi-6*p* bands are much wider. Regardless of magnetic configuration and magnetic easy axis, the calculated spin moment is around  $0.98 \mu_B$ , indicating that the Ce in  $\text{CePdBi}_2$  is trivalent. On the other hand, the calculated orbital moment is around  $-1.55 \mu_B$ , which is considerably smaller than that of a free  $\text{Ce}^{3+}$  ion, clearly illustrating the importance of CEF effects in  $\text{CePdBi}_2$ .

The Pd-4*d* bands are almost fully occupied and have only a small contribution to the Fermi energy. We thus performed virtual crystal approximation calculations by adding holes into the unit cell as a uniform background to simulate the effect of Pd vacancies [36]. As shown in Fig. 9(b), the major effect is a downshift of the Fermi level. Our calculations found that the magnetic easy axis of  $\text{CePd}_{0.78}\text{Bi}_2$  now becomes [001], which is consistent with our experimental measurements, and the magnetic configuration of  $\text{CePd}_{0.78}\text{Bi}_2$  is still A-AFM. As shown in Fig. 9(b), doping does not change the valence of Ce, and the numerical spin moment remains around  $1 \mu_B$  ( $0.97 \mu_B/\text{Ce}$ ). Doping, however, enhances the CEF effects, and consequently the orbital moment of  $\text{CePd}_{0.78}\text{Bi}_2$  is quenched to  $0.81 \mu_B$ . As mentioned above, the energy of CEF is around 75 K, which is comparable with that of  $\text{CeMSb}_2$  ( $M = \text{Cu, Au, and Ni}$ ) [16]. When the temperature is lower than the CEF energy, the orbital moment will be quenched as shown in the DFT calculations, and the magnetic behavior will deviate from the Curie-Weiss law. This agrees with

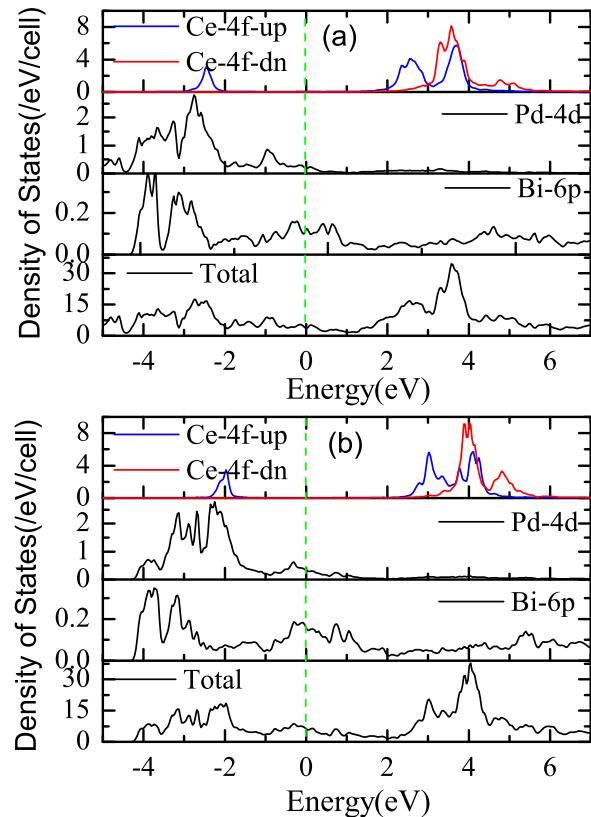


FIG. 9. (Color online) Electronic density of states (DOS) from LDA+ $U$ +SO calculations. Fermi energy  $E_F$  is set to zero. (a)  $\text{CePdBi}_2$ : A-AFM with [110] easy axis. (b)  $\text{CePd}_{0.78}\text{Bi}_2$ : A-AFM with [001] easy axis.

our experimental magnetic susceptibility data and is also consistent with the observed Fermi-surface reconstruction around 75 K.

## IV. CONCLUSIONS

The layered compound  $\text{CePd}_{1-x}\text{Bi}_2$  shows antiferromagnetic Kondo-lattice behavior. In  $\text{CePd}_{1-x}\text{Bi}_2$ , the results of resistivity, magnetoresistance, and Hall effect jointly reveal a conventional-metal behavior above 75 K and a strong interplay between Kondo and CEF effects below 75 K. The coexistence and competition of Kondo and RKKY interactions as well as CEF effects in  $\text{CePd}_{1-x}\text{Bi}_2$  quench any potential superconductivity such as the one found in  $\text{LaPd}_{1-x}\text{Bi}_2$  [5]. In other words, the Fermi-surface topology of  $\text{LaPd}_{1-x}\text{Bi}_2$  is very important to its superconductivity. The strength of *f-d* hybridization (or the degree of delocalization of the *f* electrons) in  $\text{CePd}_{1-x}\text{Bi}_2$  is moderate. This moderate strength induces a Kondo interaction in  $\text{CePd}_{1-x}\text{Bi}_2$  but is not enough to eliminate the RKKY interaction, so that the local-moment ordering occupies the ground state. The Fermi-surface reconstruction caused by Kondo and CEF effects and the magnetic ordering induced by RKKY interaction make the heavy-fermion superconductivity, such as in  $\text{CeCu}_2\text{Si}_2$  [37], have no chance to emerge. However, the possibility of pressure-induced superconductivity exists around the quantum critical point where the AFM ordering vanishes simultaneously.

## ACKNOWLEDGMENTS

This work is supported by UChicago Argonne, LLC, operator of Argonne National Laboratory, a US Department of

Energy Office of Science Laboratory operated under Contract No. DE-AC02-06CH11357. Work done at Nanjing University (by X.W.) is supported by the NSF of China (Grants No. 11374137, No. 91122035, and No. 11174124).

- 
- [1] S. Doniach, *Physica B and C* **B91**, 231 (1977).
- [2] Y. Onuki, Y. Shimizu, and T. Komatsubara, *J. Phys. Soc. Jpn.* **53**, 1210 (1984).
- [3] B. Barbara, J. X. Boucherle, J. L. Buevoz, M. F. Rossignol, and J. Schweizer, *Solid State Commun.* **24**, 481 (1977).
- [4] T. Komatsubara, T. Suzuki, M. Kawakami, S. Kunii, T. Fujita, Y. Ishikawa, A. Takase, K. Kojima, M. Suzuki, and T. Kasuya, *J. Magn. Magn. Mater.* **15–18**, 963 (1980).
- [5] F. Han, C. D. Malliakas, C. C. Stoumpos, M. Sturza, H. Claus, D. Y. Chung, and M. G. Kanatzidis, *Phys. Rev. B* **88**, 144511 (2013).
- [6] M. G. Kanatzidis, R. Pöttgen, and W. Jeitschko, *Angew. Chem. Int. Ed.* **44**, 6996 (2005).
- [7] M. A. Zhuravleva, X. Z. Chen, X. Wang, A. J. Schultz, J. Ireland, C. K. Kannewurf, and M. G. Kanatzidis, *Chem. Mater.* **14**, 3066 (2002).
- [8] Computer code X-AREA (Stoe & Cie, Darmstadt, Germany, 2002).
- [9] G. M. Sheldrick, *Acta Crystallogr.* **A64**, 112 (2008).
- [10] R. Bachmann, F. J. DiSalvo, T. H. Geballe, R. L. Greene, R. E. Howard, C. N. King, H. C. Kirsch, K. N. Lee, R. E. Schwall, H. U. Thomas, and R. B. Zubeck, *Rev. Sci. Instrum.* **43**, 205 (1972).
- [11] H. Y. Hwang, B. Batlogg, H. Takagi, H. L. Kao, J. Kwo, R. J. Cava, J. J. Krajewski, and W. F. Peck, Jr., *Phys. Rev. Lett.* **72**, 2636 (1994).
- [12] Y. Kamihara, T. Watanabe, M. Hirano, and H. Hosono, *J. Am. Chem. Soc.* **130**, 3296 (2008).
- [13] J. Paglione and R. L. Greene, *Nat. Phys.* **6**, 645 (2010).
- [14] S. W. Kim, K. Lee, D. T. Adroja, F. Demmel, J. W. Taylor, and M. H. Jung, *J. Appl. Phys.* **116**, 073901 (2014).
- [15] K. Kodama, S. Wakimoto, N. Igawa, S. Shamoto, H. Mizoguchi, and H. Hosono, *Phys. Rev. B* **83**, 214512 (2011).
- [16] A. Thamizhavel, T. Takeuchi, T. Okubo, M. Yamada, R. Asai, S. Kirita, A. Galatanu, E. Yamamoto, T. Ebihara, Y. Inada, R. Settai, and Y. Onuki, *Phys. Rev. B* **68**, 054427 (2003).
- [17] K. W. H. Stevens, *Proc. Phys. Soc. A* **65**, 209 (1952).
- [18] K. W. H. Stevens, *Rep. Prog. Phys.* **30**, 189 (1967).
- [19] K. W. H. Stevens, *Phys. Rep.* **24**, 1 (1976).
- [20] N. P. Kolmakova, I. B. Krynetskii, M. M. Lukina, and A. A. Mukhin, *Phys. Status Solidi B* **159**, 845 (1990).
- [21] J. B. Gruber, S. Chandra, D. K. Sardar, U. V. Valiev, N. I. Juraeva, and G. W. Burdick, *J. Appl. Phys.* **105**, 023112 (2009).
- [22] H. Mizoguchi, S. Matsuishi, M. Hirano, M. Tachibana, E. Takayama-Muromachi, H. Kawaji, and H. Hosono, *Phys. Rev. Lett.* **106**, 057002 (2011).
- [23] D. A. Sokolov, M. C. Aronson, C. Henderson, and J. W. Kampf, *Phys. Rev. B* **76**, 075109 (2007).
- [24] P. K. Das, N. Kumar, R. Kulkarni, and A. Thamizhavel, *Phys. Rev. B* **83**, 134416 (2011).
- [25] C. D. Bredl, F. Stglich, and K. D. Schotte, *Z. Phys. B* **29**, 327 (1978).
- [26] M. H. Jung, A. H. Lacerda, and T. Takabatake, *Phys. Rev. B* **65**, 132405 (2002).
- [27] V. K. Pecharsky, K. A. Gschneidner, Jr., and L. L. Miller, *Phys. Rev. B* **43**, 10906 (1991).
- [28] Z. Hossain, S. Hamashima, K. Umeo, T. Takabatake, C. Geibel, and F. Steglich, *Phys. Rev. B* **62**, 8950 (2000).
- [29] Z. Hossain, H. Ohmoto, K. Umeo, F. Iga, T. Suzuki, T. Takabatake, N. Takamoto, and K. Kindo, *Phys. Rev. B* **60**, 10383 (1999).
- [30] B. Cornut and B. Coqblin, *Phys. Rev. B* **5**, 4541 (1972).
- [31] A. B. Pippard, *Magnetoresistance in Metals* (Cambridge University Press, Cambridge, 1989).
- [32] M. K. Chan, M. J. Veit, C. J. Dorow, Y. Ge, Y. Li, W. Tabis, Y. Tang, X. Zhao, N. Barišić, and M. Greven, *Phys. Rev. Lett.* **113**, 177005 (2014).
- [33] S. Y. Savrasov, *Phys. Rev. B* **54**, 16470 (1996).
- [34] V. I. Anisimov, F. Aryasetiawan, and A. I. Lichtenstein, *J. Phys.: Condens. Matter* **9**, 767 (1997).
- [35] T. Jeong, *Physica B* **388**, 249 (2007).
- [36] We reduce the number of electrons in the system to simulate the hole doping, while we also change the nuclear charge of the Pd atom to make sure the system is in a neutral environment.
- [37] F. Steglich, J. Aarts, C. D. Bredl, W. Lieke, D. Meschede, W. Franz, and H. Schäfer, *Phys. Rev. Lett.* **43**, 1892 (1979).